

Supersolid-like square- and honeycomb-lattice crystallization of droplets in a dipolar condensate

Luis E. Young-S.^{1*} and S. K. Adhikari^{2†}

¹*Grupo de Modelado Computacional, Facultad de Ciencias Exactas y Naturales, Universidad de Cartagena, 130014 Cartagena, Bolívar, Colombia and*

²*Instituto de Física Teórica, UNESP - Universidade Estadual Paulista, 01.140-070 São Paulo, São Paulo, Brazil*

We demonstrate a supersolid-like spatially-periodic square- and honeycomb-lattice crystallization of droplets, in addition to the commonly-studied triangular-lattice crystallization, in a cylindrically-symmetric quasi-two-dimensional trapped dipolar condensate, using a beyond-mean-field model including a quantum-fluctuation Lee-Huang-Yang-type interaction. These three types of crystallization of droplets may appear for the *same* atomic interactions and the *same* trap frequencies. The energy E of all three crystallization as a function of number N of atoms satisfy the universal scaling relation $E \sim N^{0.4}$ indicating that all three arrangements of the droplets should be energetically probable processes of phenomenological interest. The state of square-lattice crystallization may have the central site occupied or unoccupied, corresponding to a parity-symmetric or parity-antisymmetric state, respectively. The state of square-lattice crystallization with the occupied central site and the state of triangular-lattice crystallization, for a fixed N , constitute two quasi-degenerate ground states while the other states are low-lying excited states. This makes the square-lattice crystallization with the occupied central site an ideal candidate for future experimental observation.

I. INTRODUCTION

A supersolid [1–6] is a special form of quantum matter, which exhibits a spatially-ordered stable structure, as encountered in a solid crystal, breaking continuous translational invariance. A supersolid can also flow without friction as a superfluid breaking continuous gauge invariance. Hence, contrary to the wisdom that a frictionless flow is an exclusive property of a superfluid, a supersolid simultaneously possesses the properties of a superfluid and a solid. The search of supersolidity in ^4He [7] was not conclusive [8]. However, there had been theoretical suggestions for creating a supersolid in a dipolar Bose-Einstein condensate (BEC) [9–11], in a BEC with finite-range atomic interaction [12] and in a spin-orbit (SO) coupled spinor BEC [13]. The study of a supersolid has recently gained new impetus among research workers in low-temperature physics, after the experimental observation of supersolids in a dipolar BEC [14, 15] and in an SO-coupled pseudo spin-1/2 spinor BEC [16].

Recently, a spatially-periodic state, displaying a stripe pattern in density, known as a superstripe state, because of its supersolid-like properties, was experimentally observed in an SO-coupled pseudo spin-1/2 BEC of ^{23}Na atoms [16]. In a quasi-two-dimensional (quasi-2D) uniform and trapped SO-coupled spin-2 [17], spin-1 [18, 19], and pseudo spin-1/2 [20] spinor BEC, the formation of a supersolid-like *square- and triangular-lattice* patterns in density was demonstrated in theoretical studies in addition to the superstripe state [13, 16]. In a strongly dipolar BEC, for an appropriate mixture of dipolar and contact interactions, and for the number of atoms N be-

yond a critical value, high-density droplet formation was observed experimentally in a dipolar BEC under a strong trap of ^{164}Dy [15] and ^{168}Er [21] atoms and studied theoretically [22, 23]. In the framework of a mean-field model employing the Gross-Pitaevskii (GP) equation, a dipolar BEC collapses for a strong dipolar interaction beyond a critical value, and a Lee-Huang-Yang-type [24] (LHY-type) beyond-mean-field quantum-fluctuation interaction [25, 26] is necessary in theoretical studies to stabilize a strongly dipolar droplet against collapse [11]. As the number of atoms N in a trapped dipolar BEC is increased, so that the density of atoms reaches a critical value, due to the dipolar interaction, the condensate shrinks to a very small size. However, it cannot collapse due to the quantum-fluctuation LHY interaction and a droplet is formed. The size of the droplet is much smaller than the harmonic oscillator trap lengths. Such droplets can accommodate a maximum number of atoms [22] for given harmonic trap frequencies so as to attain a critical density of atoms in the condensate. In spite of the name droplet, the present dipolar BEC droplets in a strong trap are different from recently observed [27, 28] nondipolar binary BEC droplets in free space. Nevertheless, in both cases, the collapse is arrested by a beyond-mean-field quantum-fluctuation LHY interaction.

For a sufficiently large N , in a quasi-one-dimensional (quasi-1D) trapped dipolar BEC, a spontaneous periodic crystallization of droplets along a straight line was observed in different experiments on ^{164}Dy [29–31], ^{162}Dy [32–34], and ^{166}Er [30, 31] atoms and confirmed in related theoretical studies [35, 36], whereas in a quasi-2D trapped dipolar BEC of ^{164}Dy atoms, a crystallization of droplets on a periodic triangular lattice was observed experimentally [14, 37] and established in theoretical studies [38–42]. In addition to this periodic triangular-lattice state, in a trapped quasi-2D dipolar BEC, the formation of honeycomb, stripe and other periodic structures

*lyoung@unicartagena.edu.co

†sk.adhikari@unesp.br, professores.ift.unesp.br/sk.adhikari/

in density, and not crystallization of droplets, have also been predicted [40–43] in theoretical studies. Nevertheless, in many of these investigations, specially in the numerical studies on a truncated finite system, the supersolidity of the system has never been rigorously established [44]. One needs to show the spontaneous breaking of gauge symmetry (that gives the superfluid order parameter) and the spontaneous breaking of translational symmetry in the same system. Lacking a rigorous demonstration of supersolidity, we prefer to call these periodic states supersolid-like states in this paper as in similar studies on quasi-2D SO-coupled spinor BECs [17, 19].

Following the 1D crystallization of dipolar droplets along a straight line in a quasi-1D trap [29–36], the natural crystallization in 2D is the square-lattice arrangement of droplets – not yet observed in experiments and not predicted theoretically. In this paper, using a beyond mean-field model including the quantum-fluctuation LHY interaction [25, 26] for a three-dimensional (3D) trapped dipolar BEC, we explicitly demonstrate a supersolid-like spatially-periodic square- and honeycomb-lattice crystallization of droplets in the $x-y$ plane, perpendicular to the polarization z direction, for an appropriate mixture of dipolar and contact interactions in a quasi-2D trap in addition to the triangular-lattice crystallization of droplets found in different theoretical [38, 40] and experimental [14, 37] investigations. We found that the symmetry of the final state is sensitive to the initial state employed in numerical simulation. A final state with a specific symmetry – a square, triangular, or a honeycomb lattice – can be easily obtained with the use of an initial state with the same symmetry. No such supersolid-like state can be obtained in a trapped BEC with isotropic contact interaction. In case of dipolar interaction, a single droplet can be stable for a maximum number of atoms. As the number of atoms is increased further, multiple droplets are generated and due to an interplay between the dipolar repulsion in the $x-y$ plane and the external trapping potential, a supersolid-like arrangement of droplets is formed.

In this study we find two distinct types of square-lattice arrangements of dipolar droplets in a circularly-symmetric quasi-2D trapped dipolar BEC, e.g., with the central site at $x = y = 0$ occupied or vacant. In the case, the central site is occupied (unoccupied) by a droplet the wave function is parity-symmetric (parity-antisymmetric). In the first type we find 9, 25, and 49... droplets arranged on 3×3 , 5×5 , 7×7 ... arrays, whereas in the second type we find 4, 16, 36... droplets arranged on 2×2 , 4×4 , 6×6 ... arrays as in Fig. 2. Like usual parity-antisymmetric states, square-lattice crystallization with a vacant central site is an excited state. We also numerically investigate the triangular-lattice arrangement of droplets studied previously. In addition to the triangular and square-lattice arrangements, we also demonstrate a clean honeycomb-lattice arrangement of droplets. A honeycomb lattice is a special case of a triangular lattice with missing droplets at the centers of adjacent

hexagons. Of these different possibilities, the triangular-lattice arrangement of droplets and the square-lattice arrangement with an occupied central site constitute two quasi-degenerate stable ground states. The honeycomb-lattice and the square-lattice arrangements with a vacant central site have slightly larger energies and are excited states.

We also calculated the energies of the different states and established a universal scaling relation between the energy per atom E of the supersolid-like crystallization of droplets on square, honeycomb and triangular lattices and the number of atoms N , independent of the type of lattice, which implies that these three periodic crystallization of droplets are all equally probable energetically. Moreover, the three different crystallization of droplets appear for the same atomic contact and dipolar interactions and for the same trap frequencies. Hence all these periodic crystallization of droplets should be of experimental interest. With this in mind, in this paper, we have employed the same confining trap frequencies and similar number of ^{164}Dy atoms as in previous experimental [37] and theoretical [38] studies on the triangular lattice formation of dipolar droplets. The number of droplets n_d is found to increase approximately linearly with N .

In Sec. II we present the beyond-mean-field model including the quantum-fluctuation LHY interaction in the GP equation. The time-independent version of this equation is also obtained from a variational rule using a time-independent energy functional. In Sec. III we present the numerical results for stationary states with three types of periodic array of droplets, e.g. square lattice, triangular lattice and honeycomb lattice, in a trapped dipolar BEC. Finally, in Sec. IV we present a summary of our findings.

II. BEYOND-MEAN-FIELD MODEL

In this paper we base our study on a 3D beyond-mean-field model including the quantum-fluctuation LHY interaction. We consider a BEC of N dipolar atoms polarized along the z axis, of mass m each, interacting through the following atomic dipolar and contact interactions [45–47]

$$V(\mathbf{R}) = \frac{\mu_0 \mu^2}{4\pi} \frac{1 - 3 \cos^2 \theta}{|\mathbf{R}|^3} + \frac{4\pi \hbar^2 a}{m} \delta(\mathbf{R}), \quad (1)$$

where a is the scattering length, μ_0 is the permeability of vacuum, μ is the magnetic dipole moment of each atom, $\mathbf{R} = \mathbf{r} - \mathbf{r}'$ is the vector joining two dipoles placed at $\mathbf{r} \equiv \{\mathbf{x}, \mathbf{y}, \mathbf{z}\}$ and $\mathbf{r}' \equiv \{\mathbf{x}', \mathbf{y}', \mathbf{z}'\}$ and θ is the angle made by \mathbf{R} with the z axis. The strength of dipolar interaction is given by the dipolar length

$$a_{\text{dd}} = \frac{\mu_0 \mu^2 m}{12\pi \hbar^2}. \quad (2)$$

The dimensionless ratio

$$\varepsilon_{\text{dd}} \equiv \frac{a_{\text{dd}}}{a} \quad (3)$$

determines the strength of the dipolar interaction relative to the contact interaction and controls many properties of a dipolar BEC.

A dipolar BEC is described by the following 3D beyond-mean-field GP equation including the quantum-fluctuation LHY interaction [23, 38, 45–47]

$$i\hbar\frac{\partial\psi(\mathbf{r},t)}{\partial t} = \left[-\frac{\hbar^2}{2m}\nabla^2 + U(\mathbf{r}) + \frac{4\pi\hbar^2}{m}aN|\psi(\mathbf{r},t)|^2 + \frac{3\hbar^2}{m}a_{\text{dd}}N\int\frac{1-3\cos^2\theta}{|\mathbf{R}|^3}|\psi(\mathbf{r}',t)|^2d\mathbf{r}' + \frac{\gamma_{\text{QF}}\hbar^2}{m}|\psi(\mathbf{r},t)|^3 \right] \psi(\mathbf{r},t), \quad (4)$$

where $U(\mathbf{r}) = \frac{1}{2}m(\omega_x^2x^2 + \omega_y^2y^2 + \omega_z^2z^2)$ is the trap with angular frequencies $\omega_x \equiv 2\pi f_x$, $\omega_y \equiv 2\pi f_y$, $\omega_z \equiv 2\pi f_z$ along x, y, z directions, respectively, the wave function is normalized as $\int|\psi(\mathbf{r},t)|^2d\mathbf{r} = 1$. The coefficient of the beyond-mean-field quantum-fluctuation LHY term γ_{QF} is given by [23, 25, 26]

$$\gamma_{\text{QF}} = \frac{128}{3}\sqrt{\pi a^5}Q_5(\varepsilon_{\text{dd}}), \quad (5)$$

where the auxiliary function

$$Q_5(\varepsilon_{\text{dd}}) = \int_0^1 dx(1-x+3x\varepsilon_{\text{dd}})^{5/2} \quad (6)$$

can be evaluated as [23]

$$Q_5(\varepsilon_{\text{dd}}) = \frac{(3\varepsilon_{\text{dd}})^{5/2}}{48}\text{Re}\left[(8+26\varepsilon+33\varepsilon^2)\sqrt{1+\varepsilon} + 15\varepsilon^3\ln\left(\frac{1+\sqrt{1+\varepsilon}}{\sqrt{\varepsilon}}\right)\right], \quad \varepsilon = \frac{1-\varepsilon_{\text{dd}}}{3\varepsilon_{\text{dd}}}, \quad (7)$$

$$\approx 1 + \frac{3}{2}\varepsilon_{\text{dd}}^2 \quad (8)$$

where Re denotes the real part. In the present study we use the exact expression (7). The use of the approximate expression (8), as, for example, in Refs. [39, 42], leads to qualitatively acceptable results for droplet and droplet-lattice formation, but may lead to sizable error in quantitative estimate of energy, size, etc. of the final state.

Equation (4) can be reduced to the following dimensionless form by scaling lengths in units of $l = \sqrt{\hbar/m\omega_z}$, time in units of ω_z^{-1} , energy in units of $\hbar\omega_z$, and density $|\psi|^2$ in units of l^{-3}

$$i\frac{\partial\psi(\mathbf{r},t)}{\partial t} = \left[-\frac{1}{2}\nabla^2 + \frac{1}{2}\left(\frac{f_x^2}{f_z^2}x^2 + \frac{f_y^2}{f_z^2}y^2 + z^2\right) + 3a_{\text{dd}}N\int\frac{1-3\cos^2\theta}{|\mathbf{R}|^3}|\psi(\mathbf{r}',t)|^2d\mathbf{r}' + 4\pi aN|\psi(\mathbf{r},t)|^2 + \gamma_{\text{QF}}N^{3/2}|\psi(\mathbf{r},t)|^3 \right] \psi(\mathbf{r},t). \quad (9)$$

Equation (9) can also be obtained from the variational rule

$$i\frac{\partial\psi}{\partial t} = \frac{\delta E}{\delta\psi^*} \quad (10)$$

with the following energy functional (energy per atom)

$$E = \int d\mathbf{r} \left[\frac{|\nabla\psi(\mathbf{r})|^2}{2} + \frac{1}{2}\left(\frac{f_x^2}{f_z^2}x^2 + \frac{f_y^2}{f_z^2}y^2 + z^2\right)|\psi(\mathbf{r})|^2 + \frac{3}{2}a_{\text{dd}}N|\psi(\mathbf{r})|^2\int\frac{1-3\cos^2\theta}{R^3}|\psi(\mathbf{r}')|^2d\mathbf{r}' + 2\pi Na|\psi(\mathbf{r})|^4 + \frac{2\gamma_{\text{QF}}}{5}N^{3/2}|\psi(\mathbf{r})|^5 \right] \quad (11)$$

for a stationary state.

III. NUMERICAL RESULTS

We solve partial differential equation (9) for a dipolar BEC numerically, using FORTRAN/C programs [46] or their open-multiprocessing versions [48], by the split-time-step Crank-Nicolson method [49] employing the imaginary-time propagation rule. Often, the intensity of the system has large extension in the $x-y$ plane and it is appropriate to take a larger number of discretization steps along x and y directions as compared to the same along the z direction. It is problematic to treat numerically the nonlocal dipolar interaction integral in the beyond-mean-free model (9) in configuration space due to the $1/|\mathbf{R}|^3$ term. To circumvent the problem, this term is evaluated in the momentum space by a Fourier transformation using a convolution identity [46], which is advantageous numerically due to the smooth behavior of this term in momentum space. The Fourier transformation of the dipolar potential in 3D can be found analytically enhancing the accuracy of the numerical procedure.

Instead of presenting results in dimensionless units, we prefer to relate our results to the recent experimental [37] and related theoretical [38] studies on dipolar droplets using ^{164}Dy atoms. For the appearance of droplets we need a strongly dipolar atom with $\varepsilon_{\text{dd}} > 1$ necessarily [14]. In this study we take $a = 85a_0$, close to its experimental estimate $a = (92 \pm 8)a_0$ [50], and $a_{\text{dd}} = 130.8a_0$, where a_0 is the Bohr radius; consequently, $\varepsilon_{\text{dd}} = 1.5388... > 1$. This value of scattering length is close to the scattering lengths $a = 88a_0$ [37, 38] and $a = 70a_0$ [39] used in some other studies of quantum droplets in a quasi-2D dipolar BEC. The trap frequencies along x, z , and y directions are taken as $f_x = 33$ Hz, $f_z = 167$ Hz, and $f_y = 110$ Hz (trap U_A), $= 60$ Hz (trap U_B), $= 33$ Hz (trap U_C) as in recent experimental [37] and theoretical [38] investigations on triangular-lattice crystallization of droplets. The trap U_A is of quasi-1D type along the x direction ($f_y, f_z \gg f_x$) and the trap U_C it is of a cylindrically-symmetric quasi-2D type in the $x-y$ plane ($f_x = f_y \ll f_z$). The trap U_B is an asymmetric trap ($f_x \neq f_y \neq f_z$) in the transition domain from a quasi-1D to a quasi-2D type. With these parameters – frequencies for trap U_C and scattering length a – we found simultaneously square-, triangular-, and honeycomb-lattice crystallization of droplets in a trapped quasi-2D dipolar BEC of ^{164}Dy atoms and these three different arrangements of

droplets are found to have similar energies for a fixed N . In this study we have $m(^{164}\text{Dy}) = 164 \times 1.66054 \times 10^{-27}$ kg, $\hbar = 1.0545718 \times 10^{-34}$ m² kg/s, $\omega_z = 2\pi \times 167$ Hz, consequently, unit of length $l = \sqrt{\hbar/m\omega_z} = 0.607$ μm .

For an efficient and quick convergence of a single-droplet state or of a lattice-droplet arrangement in an imaginary-time calculation, an appropriate choice of the initial state is essential. The numerical simulation of a single-droplet state was started with a Gaussian wave function of small width: $\phi(\mathbf{r}) \sim e^{-x^2-y^2}e^{-z^2/\alpha^2}$, with the width parameter $\alpha \approx 4$. The numerical simulation for a lattice-droplet state was started by many Gaussian droplets arranged on a desired lattice. For example, a 49-droplet square-lattice state, viz. Fig. 3(f), was started with the following analytic function

$$\phi(\mathbf{r}) \sim \sum_{i,j=0}^{\pm 1, \pm 2, \pm 3} e^{-(x+\beta i)^2 - (y+\beta j)^2} e^{-z^2/\alpha^2}, \quad (12)$$

with the lattice length $\beta \approx 5$. The calculation with a honeycomb- and triangular-lattice states were initiated similarly using analytic initial functions with the droplets arranged appropriately.

To find an 1D crystallization of droplets, we consider 25000 ^{164}Dy atoms in the quasi-1D trap U_A . With this trap $f_x \ll f_y, f_z$, the dipolar BEC crystallizes in droplets along the x axis. The converged final state in this case can be obtained by imaginary-time simulation using an initial Gaussian wave function. However, the convergence is quicker if we use an analytic wave function for a few droplets (3 or 5) periodically arranged along the x direction with a mutual separation β and symmetrically placed around the occupied $x = 0$ site. A contour plot of the $z = 0$ section of the 3D density $|\psi(x, y, 0)|^2$ is shown in Fig. 1(a) with 3 droplets placed symmetrically around $x = 0$ (a parity-symmetric state). For the same set of parameters, there is a parity-antisymmetric excited state of higher energy with four droplets placed symmetrically around $x = 0$, but with the central site at $x = 0$ unoccupied (not shown here), viz. Fig. 1(a) of Ref. [38]. In trap U_B , as trap frequency f_y is reduced to 60 Hz, the number of droplets for $N = 25000$ reduces from 3 to 1 as shown in Fig. 1(b), where we use the final converged wave function of Fig. 1(a) as the initial state in the imaginary-time simulation. A droplet will be formed when the density is larger than a critical density. Inside a droplet the dipolar interaction is so strong that the dipolar BEC becomes quasi-1D along the z direction with a small transverse section. A weaker trap in Fig. 1(b), compared to the same in Fig. 1(a), requires a larger number of atoms to attain the critical density required for droplet formation [40]. Consequently, a droplet in the weaker trap U_B can accommodate a larger number of atoms and the number of droplets is reduced from 3 in trap U_A to 1 in trap U_B . In the cylindrically-symmetric quasi-2D weak trap U_C , the central density for 25000 atoms is smaller than the threshold for droplet formation; consequently, no droplets can be formed and the

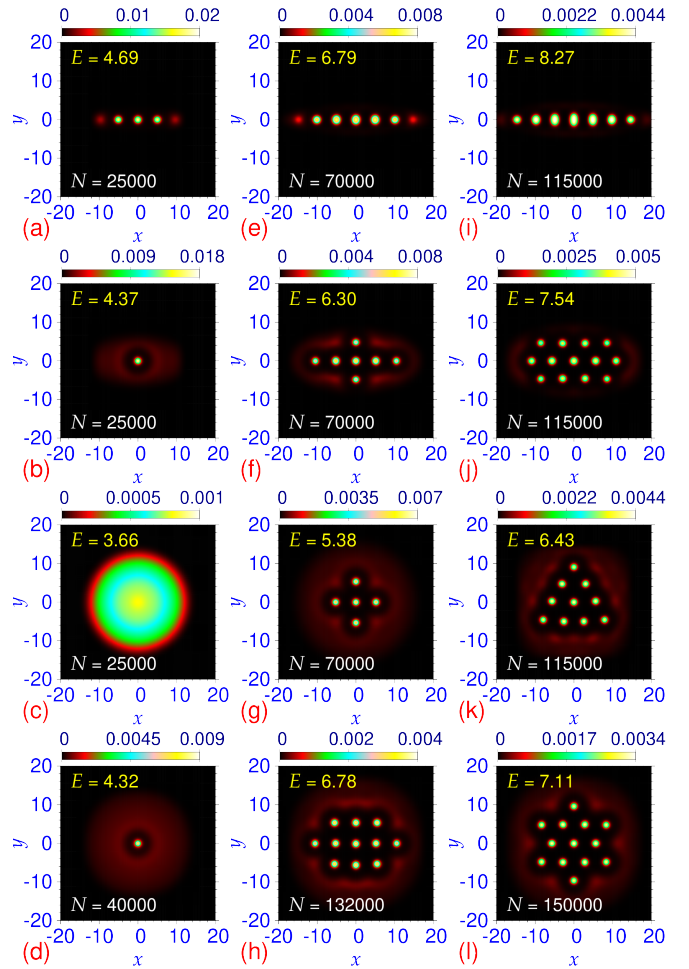


FIG. 1: Contour plot of density $|\psi(x, y, 0)|^2$ of a dipolar BEC of $N = 25000$ ^{164}Dy atoms in trap (a) U_A ($f_y = 110$ Hz), (b) U_B ($f_y = 60$ Hz) and (c) U_C ($f_y = 33$ Hz); the same of $N = 40000$ atoms in trap (d) U_C ; the same of $N = 70000$ atoms in trap (e) U_A , (f) U_B and (g) U_C ; the same of $N = 132000$ atoms in trap (h) U_C ; the same of $N = 115000$ atoms in trap (i) U_A , (j) U_B and (k) U_C ; the same of $N = 150000$ atoms in trap (l) U_C . All plots are labelled by respective E and N values. In the first column we illustrate the formation of a single droplet, in the second column the formation of square-lattice arrangement of droplets and in the third column that of triangular-lattice arrangement of droplets. Other parameters in all calculations are $f_x = 33$ Hz, $f_z = 167$ Hz, $a = 85a_0$, $a_{\text{dd}} = 130.8a_0$. Plotted quantities in all figures are dimensionless; the length scale $l \equiv \sqrt{\hbar/m\omega_z} = 0.607$ μm .

density is of normal Gaussian type, viz. Fig. 1(c), with a large increase in the size of the condensate. However, for $N > N_{\text{cr}} = 33000$ the critical density for the formation of droplet is attained in trap U_C and a droplet can be formed as shown in Fig. 1(d) for $N = 40000$.

We illustrate the quasi-1D to quasi-2D transition of square-lattice arrangement of droplets for a fixed number of atoms $N = 70000$ in Figs. 1(e)-(g) for traps U_A ,

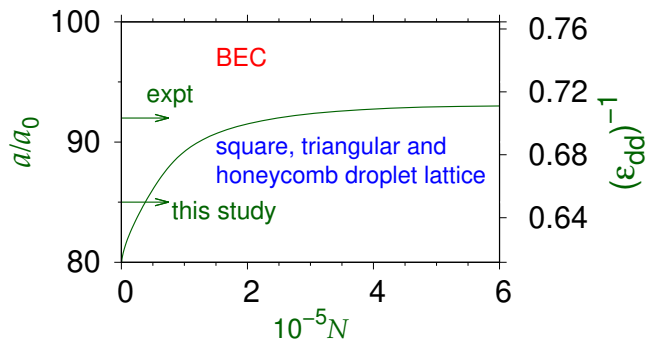


FIG. 2: The a/a_0 versus N phase plot of droplet formation in trap U_C illustrating the square-, triangular- and honeycomb-lattice states. The region marked “BEC” represents a normal BEC of the type displayed in Fig. 1(c), where no droplet can be formed.

U_B and U_C , respectively, through a contour plot of 2D density $|\psi(x, y, 0)|^2$ in the $x - y$ plane. In the quasi-1D trap U_A , we have a linear chain of droplets in Fig. 1(e) and, in the quasi-2D trap U_C , an $x - y$ symmetric arrangement of droplets is obtained as shown in Fig. 1(g). An arrangement of droplets in the quasi-1D to quasi-2D transition domain in trap U_B is illustrated in Fig. 1(f). The number of droplets in a specific trap increases with N as shown in Fig. 1(h) for $N = 132000$ in trap U_C with 11 droplets compared to 5 droplets in Fig. 1(g) for $N = 70000$.

The quasi-1D to quasi-2D transition of triangular-lattice arrangement of droplets for $N = 115000$ in Figs. 1(i)-(k) for traps U_A , U_B and U_C , respectively, is considered next through a contour plot of 2D density $|\psi(x, y, 0)|^2$ in the $x - y$ plane. In the quasi-1D trap U_A again we have a linear array of droplets in Fig. 1(i) and a triangular lattice of droplets in the quasi-2D trap U_C is displayed in Fig. 1(k). An intermediate triangular-lattice arrangement of droplets in trap U_B in the transition from quasi-1D to quasi-2D is presented in Fig. 1(j). In a quasi-1D trap U_A , the number of droplets n_d increases with N , as can be found from Figs. 1(a), (e) and (i). In the quasi-2D trap U_C , in general n_d also increases with N , viz. Figs. 1(g), (k), (h), and (l) with 5, 10, 11, 13 droplets for $N = 70000, 115000, 132000, 150000$, respectively. The number of droplets is roughly proportional to the number of atoms. In Figs. 1(k) and (l) we find that a triangle-shaped triangular lattice has changed to a star-shaped triangular lattice with the increase of N in the same trap U_C .

In all cases, surrounding the lattice arrangement of droplets, a cloud of atoms is found. It was not possible to avoid this cloud; if the calculation is repeated with a smaller N , the droplets at the four corners start to disappear maintaining the cloud intact. Similar cloud was also found in other theoretical [38–40] and experimental [37] investigations.

After having established the formation of dipolar

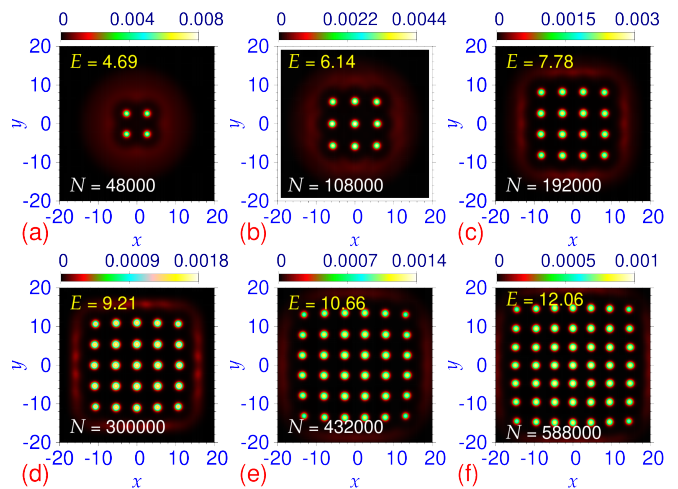


FIG. 3: Contour plot of density $|\psi(x, y, 0)|^2$ of square-lattice crystallization of 4, 9, 16, 25, 36, and 49 droplets, respectively, for (a) $N = 48000$, (b) $N = 108000$, (c) $N = 192000$, (d) $N = 300000$, (e) $N = 432000$ (f) $N = 588000$ in trap U_C .

droplets of different symmetries, we present a a/a_0 versus N phase plot for droplet formation in trap U_C , (as our study will be confined to this quasi-2D trap,) in Fig. 2, where the experimental scattering length $a = 92a_0$ [50] and the present scattering length $a = 85a_0$ are marked by arrows. This phase plot bears some similarity with the phase plot presented in Fig. 3 of Ref. [40] for $a_{\text{dd}} = 130a_0$ in spite of different trap frequencies in that reference. Although the region of droplet formation of Ref. [40] is quite similar to the same of Fig. 2, only triangular-lattice formation is reported in Ref. [40]. Here we show that it is possible to have periodic square-, honeycomb-, and triangular-lattice arrangement of droplets in the same region. The stripe and honeycomb structures (and not honeycomb-lattice droplet as reported in this paper) of Fig. 3 of Ref. [40] are possible beyond $N = 6 \times 10^5$, which is not considered in Fig. 2. In this study, we employ $a = 85a_0$ and a large N , deep inside the region of droplet formation in Fig. 2, where a large number of droplets can be formed.

To study the square-lattice crystallization of droplets in the cylindrically-symmetric quasi-2D trap U_C we note that there are two types of square-lattice crystallization – an even number of droplets on each side of the square (with $2 \times 2 = 4$, $4 \times 4 = 16$, $6 \times 6 = 36$ etc. droplets) or an odd number of droplets on each side of the square (with $3 \times 3 = 9$, $5 \times 5 = 25$, $7 \times 7 = 49$ etc. droplets);– the corresponding density $|\psi(x, y, 0)|^2$ in trap U_C is plotted in Figs. 3(a)-(f) for $N = 48000, 108000, 192000, 300000, 432000$, and 588000 , respectively. For a symmetric distribution of the droplets, in the first (second) type, the central site at $x = y = 0$ has to be vacant (occupied), corresponding to a parity-antisymmetric (parity-symmetric) state. All states are obtained by imaginary-time simulation using

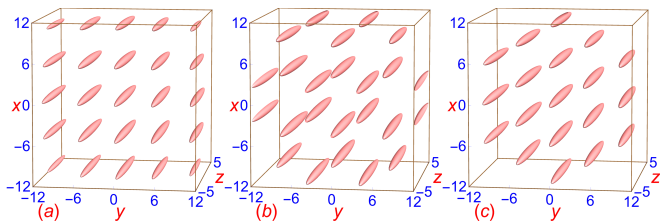


FIG. 4: Isodensity contour of 3D density $|\psi(x, y, z)|^2$ for (a) the square-lattice crystallization of Fig. 3(d) for $N = 300000$, (b) the honeycomb-lattice crystallization of Fig. 5(b) for $N = 264000$ and (c) the triangular-lattice crystallization of Fig. 6(b) for $N = 228000$ in trap U_C .

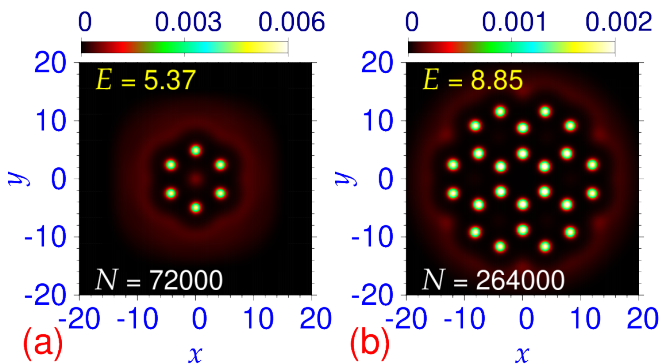


FIG. 5: Contour plot of density $|\psi(x, y, 0)|^2$ of honeycomb-lattice crystallization of droplets for (a) $N = 72000$, (b) $N = 264000$ in trap U_C .

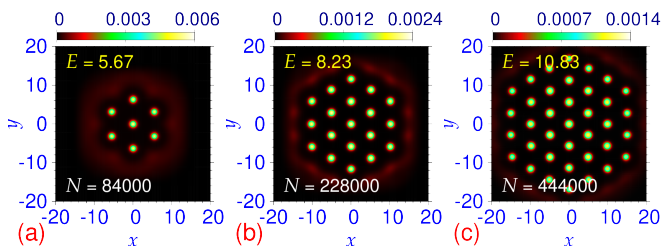


FIG. 6: Contour plot of density $|\psi(x, y, 0)|^2$ of triangular-lattice crystallization of droplets for (a) $N = 84000$, (b) $N = 228000$ and (c) $N = 444000$ in trap U_C .

an analytic initial wave function on a square lattice with lattice spacing β , viz. Eq. (12). The appropriate N per droplet in a calculation for an efficient square-lattice formation was found to be of the order of 12000. For a smaller N , the droplets at the corners may disappear and for a larger N , a intense cloud is formed around the droplets. With further increase of number of atoms, multiple (about two to four) droplets will be formed, thus reducing the cloud. In Fig. 4(a) we display the isodensity contour of density $|\psi(x, y, z)|^2$, for the square-lattice crystallization of Fig. 3(d).

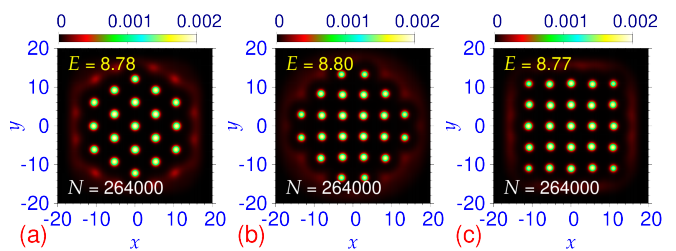


FIG. 7: Contour plot of density $|\psi(x, y, 0)|^2$ of (a) triangular-lattice crystallization, (b) square-lattice crystallization with vacant central site, and (c) square-lattice crystallization with occupied central site, for $N = 264000$, in trap U_C .

A numerical simulation of the honeycomb-lattice crystallization of droplets needed much more care than the square- and triangular-lattice arrangement of droplets. This is because this arrangement is basically a triangular-lattice arrangement of droplets with a missing droplet at the center of all closed adjacent hexagons and if the initial state is not properly chosen, the imaginary-time numerical simulation may converge to the triangular-lattice arrangement of droplets filling in the vacant positions at the center of the closed hexagons with droplets. The densities of honeycomb-lattice crystallization for 6 and 24 droplets in trap U_C are displayed in Figs. 5(a) and (b), respectively, for $N = 72000$ and 264000 . In Fig. 4(b) we present the isodensity contour of 3D density $|\psi(x, y, z)|^2$ for the honeycomb-lattice crystallization of Fig. 5(b).

Finally, we investigate the triangular-lattice crystallization of droplets in trap U_C . In Figs. 6(a), (b) and (c) we display the contour plot of density $|\psi(x, y, 0)|^2$ of triangular-lattice crystallization of 7, 19, and 37 droplets in trap U_C for $N = 84000$, 228000 and 444000 , respectively, calculated using an initial state of similar symmetry properties. In Fig. 4(c) we display the isodensity contour of density $|\psi(x, y, z)|^2$, for the triangular-lattice crystallization of Fig. 6(b).

It is pertinent to ask that, of the states of different arrangements of dipolar droplets, which is/are the ground state(s) and which are the excited states. There are two types of arrangement of droplets: the one with the central site at $x = y = 0$ occupied (square lattice with an odd number of droplets and triangular lattice) and one with the central site vacant (square lattice with an even number of droplets and honeycomb lattice). We find that the first of these types forms quasi-degenerate ground states and the second type forms low-lying excited states. To demonstrate this claim we display in Figs. 7(a)-(c) contour plot of density $|\psi(x, y, 0)|^2$ for $N = 264000$ for triangular-lattice symmetry and two types of square-lattice symmetries. We find from Figs. 6(b) and 7(a) that one can have a 19-droplet triangular-lattice state for $N = 228000$ and $N = 264000$, respectively; with an increased N in Fig. 7(a) one has an increased density of atom cloud. Similarly, in Figs. 3(d) and 7(c) one finds a 25-droplet square-lattice state for $N = 300000$

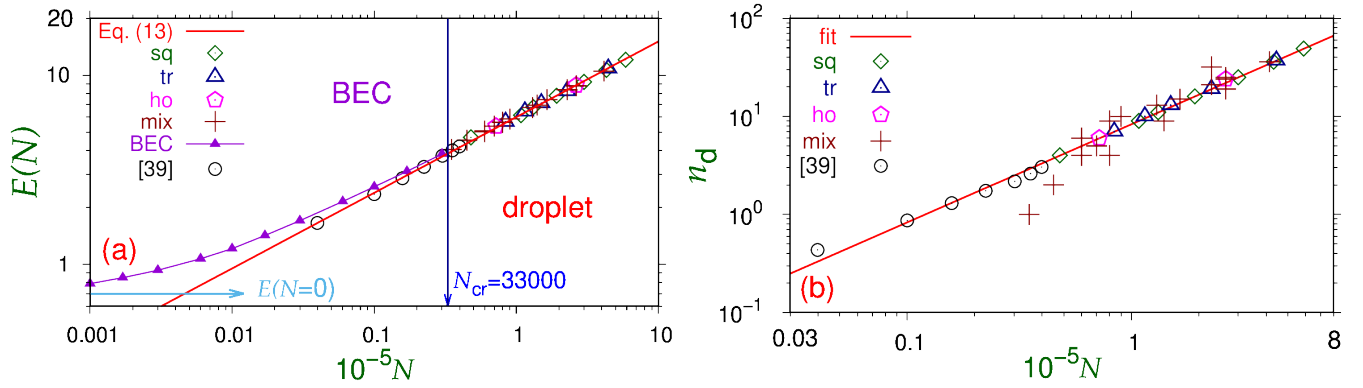


FIG. 8: (a) Energy per atom E and (b) number of droplets n_d versus N of all lattice states in trap U_C on log-log scale; sq: square-lattice states of Figs. 1(g)-(h) and 3; tr: triangular-lattice states of Figs. 1(k)-(l) and 6; ho: honeycomb-lattice states of Fig. 5; mix: the states presented in Fig. 7 and a few more not shown in this paper; BEC: normal BEC superfluid for smaller N (states of type presented in Fig. 1(c)); [39]: one- to seven-droplet states from Fig. 2(a) of [39] employing $f_x = f_y = 60$ Hz, $f_z = 300$ Hz, $a = 70a_0$, and approximation (8) in arbitrary units. The points are numerical results and the straight lines labeled (a) “Eq. (13)” and (b) “fit” are the scaling relations $E \approx 0.06 \times N^{0.4}$ and $n_d \approx N/12000$, respectively. The regions of normal BEC and droplet formation in trap U_C are marked “BEC” and “droplet”, respectively.

and $N = 264000$, respectively. In this case with larger N in Fig. 3(d) one has an increased density of atom cloud. From Figs. 7 and 5(b), for a fixed $N = 264000$, we find that the parity-symmetric square-lattice state with occupied central site, viz. Fig. 7(c), and the triangular-lattice state, viz. Fig. 7(a), constitute the quasi-degenerate ground states of energy $E = 8.77$ and $E = 8.78$, respectively. The parity-antisymmetric square-lattice state with vacant central site ($E = 8.80$), viz. Fig. 7(b), and the honeycomb-lattice state ($E = 8.85$), viz. Fig. 5(b), are low-lying excited states. Similar result was found to be true for a few other N values (details not reported in this paper). In addition to the states of droplet arrangements on periodic lattices, highlighted in this paper, there could also be states of droplet arrangements with no specific symmetry. For a specific trap and for a fixed N all these states have nearby energies (not illustrated in this paper). In addition to the quasi-degenerate stable ground states, the imaginary-time approach also finds excited states with a specific symmetry, e.g., the parity-antisymmetric square-lattice and honeycomb-lattice states, which could be metastable.

To study the universal nature of the formation of droplets for different N and different lattice symmetries in trap U_C , we plot in Fig. 8(a)-(b) the energy E per atom and the number of droplets n_d versus the corresponding N . In addition, we plot the energy from Fig. 2(a) of Ref. [39] for one- to seven-droplet states, in arbitrary units, calculated with different trap parameters ($f_x = f_y = 60$ Hz and $f_z = 300$ Hz) and a different scattering length $a = 70a_0$. We could reproduce the results of Fig. 2(a) of Ref. [39] using the approximate auxiliary function (8) in place of the exact expression (7) used in this paper. For example, using Eq. (8), for the one-droplet state of Ref. [39] we obtain the energy per

atom $E/h \approx 348$ Hz and for the seven-droplet state we obtain $E/h \approx 840$ Hz, close to the results illustrated in Fig. 2(a) of Ref. [39]. The use of Eq. (7) leads to much larger energies. From Fig. 8(a) we find the scaling relation between E and N in the region of droplet formation ($N > N_{cr} = 33000$ in trap U_C):

$$E \approx 0.06 \times N^{0.4} \quad (13)$$

independent of the lattice symmetry, scattering length a , and trap parameters. We multiplied the results of Ref. [39] by an arbitrary factor (~ 1.5) to take care of the prefactor in scaling (13), nevertheless, it is remarkable that all points lie on the same universal line and the exponent (0.4) is independent of scattering length and trap parameters. The point with the smallest number of atoms from our calculation in Fig. 8(a) is $N = 35000$ with one droplet. By including the results of Ref. [39], we could include six points with $N < 40000$ containing 1–7 droplets covering about one order of magnitude in Fig. 8(a): with the parameters of Ref. [39] one droplet can be generated with only a much smaller number $N = 3980$ of atoms. The points labelled BEC in Fig. 8(a) represent a normal superfluid BEC without droplet formation, viz. Fig. 2. These points deviate a bit from the universal scaling (13) valid for droplets, specially for small N . From Fig. 8(b), with exactly the same points of Fig. 8(a), the number of droplets n_d in an arrangement is approximately linearly proportional to N : $n_d \approx N/12000$ indicating the average number of 12000 atoms per droplet; we note that the points generating the large width of the scaling in Fig. 8(b) have collapsed on the straight-line fit (13) in Fig. 8(a). The small difference in energy between the ground and the excited states, viz. Figs. 7 and 5(b), is not noticeable in Fig. 8(a). We have established the universal nature of scaling (13) in the fact that the expo-

ment is independent of not only the value of N extended over about two orders of magnitude but also of different parameters of the problem, trap frequencies and scattering length. It remains to be seen if this exponent is independent of large variation of the dipole moment or of the details of the beyond-mean-field correction, that stops the collapse. Only after establishing the true universality, the physical origin of the scaling relation could be addressed [51], which will be an interesting topic of future investigation.

In this theoretical study we have neglected the effect of three-body recombination loss of atoms. A matter of concern for the experimental observation [15, 42] of a spatially periodic lattice of droplets is the large atom number ($N \sim 10^5$) required, where the effect of three-body recombination loss of atoms might not be negligible [40]. Nevertheless, a reasonably small value of the loss parameter ($= 1.25 \times 10^{-41}$) m^6/s is estimated for ^{164}Dy atoms [15, 29] from measurements on a thermal cloud and is assumed to be a constant over the small range of scattering lengths near $a = 60 - 80a_0$ close to the experimental estimate $a = 92a_0$ [50] and the value $a = 85a_0$ used in this study. Considering an upper estimate of $N = 10^6$ atoms of this study, viz. Figs. 3 and 4, in a volume of $40 \times 40 \times 10$ in dimensionless units with the length scale $l = 0.607 \mu\text{m}$, we obtain a typical atomic density of $3 \times 10^{14} \text{cm}^{-3} = 3 \times 10^{20} \text{m}^{-3}$ within the acceptable limit for the formation of droplets in an experiment as established in previous experimental [15, 29] and theoretical [40, 42] investigations.

IV. SUMMARY

We have demonstrated, using the GP equation including the quantum-fluctuation LHY interaction, supersolid-like spatially-periodic crystallization of droplets of a cylindrically-symmetric quasi-2D trapped dipolar BEC on square and honeycomb lattices, in addition to the triangular-lattice crystallization observed experimentally [14] and studied theoretically [38, 39]. There are two possible types of square-lattice crys-

tallization of droplets, e.g., with the central site at $x = y = 0$ occupied (parity-symmetric) or vacant (parity-antisymmetric). The parity-symmetric square-lattice crystallization and triangular-lattice crystallization form two quasi-degenerate ground states. The parity-antisymmetric square-lattice crystallization and honeycomb-lattice crystallization, both with the central site vacant, form two low-lying excited states. The number of droplets in these lattice arrangements increases with the number of atoms in an approximate linear fashion. We establish a robust scaling relation (13) valid for about two orders of magnitude between the energy per atom and the number of atoms, for number of atoms in the region of droplet formation, independent of the lattice symmetry (square, honeycomb or triangular) of droplets, so that the three lattice crystallizations should be of phenomenological interest. The stability of each of these crystallizations can be theoretically established by a linear stability analysis. However, this is a formidable task of future interest, considering the nonlocal nature of dipolar interaction. Nevertheless, both the triangular- and square-lattice structures are close-packed quasi-degenerate structures with a predominantly repulsive “inter-droplet” interaction and are expected to be stable, whereas, the excited honeycomb-lattice structure has an empty site at the center of an hexagon and is conjectured to be unstable. Hence, from an energetic consideration, the parity-symmetric square-lattice crystallization, with the central site at $x = y = 0$ occupied, is a likely candidate for experimental observation in addition to the already observed triangular-lattice crystallization. The results of this paper can be tested in experiments with strongly dipolar atomic BECs of ^{164}Dy or ^{168}Er atoms with present knowhow.

Acknowledgments

SKA acknowledges support by the CNPq (Brazil) grant 301324/2019-0, and by the ICTP-SAI FR-FAPESP (Brazil) grant 2016/01343-7

-
- [1] E. P. Gross, Phys. Rev. 106, 161 (1957).
 - [2] A. F. Andreev and I. M. Lifshitz, Zurn. Eksp. Teor. Fiz. 56, 2057 (1969) [English Transla.: Sov. Phys. JETP 29, 1107 (1969)].
 - [3] A. J. Leggett, Phys. Rev. Lett. 25, 1543 (1970).
 - [4] G. V. Chester, Phys. Rev. A 2, 256 (1970).
 - [5] M. Boninsegni and N. V. Prokofev, Rev. Mod. Phys. 84, 759 (2012).
 - [6] V. I. Yukalov, Physics 2, 49 (2020).
 - [7] E. Kim and M. H. W. Chan, Nature (London) 427, 225 (2004).
 - [8] S. Balibar, Nature (London) 464, 176 (2010).
 - [9] Z.-K. Lu, Y. Li, D. S. Petrov, and G. V. Shlyapnikov, Phys. Rev. Lett. 115, 075303 (2015).
 - [10] N. Y. Yao, C. R. Laumann, A. V. Gorshkov, S. D. Bennett, E. Demler, P. Zoller, and M. D. Lukin, Phys. Rev. Lett. 109, 266804 (2012).
 - [11] F. Wächtler and L. Santos, Phys. Rev. A 93, 061603(R) (2016).
 - [12] F. Cinti, T. Macrì, W. Lechner, G. Pupillo, and T. Pohl, Nat. Commun. 5, 3235 (2014).
 - [13] Y. Li, G. I. Martone, L. P. Pitaevskii, and S. Stringari, Phys. Rev. Lett. 110, 235302 (2013).
 - [14] H. Kadau, M. Schmitt, M. Wenzel, C. Wink, T. Maier, I. Ferrier-Barbut, and T. Pfau, Nature (London) 530, 194 (2016).

- [15] M. Schmitt, M. Wenzel, F. Böttcher, I. Ferrier-Barbut, and T. Pfau, *Nature (London)* 539, 259 (2016).
- [16] J.-R. Li, J. Lee, W. Huang, S. Burchesky, B. Shteynas, F. Ç. Top, A. O. Jamison, and W. Ketterle, *Nature (London)* 543, 91 (2017).
- [17] P. Kaur, S. Gautam, and S. K. Adhikari, *Phys. Rev. A* 105, 023303 (2022).
- [18] S. K. Adhikari, *Phys. Rev. A* 103, L011301 (2021).
- [19] S. K. Adhikari, *J. Phys.: Condens. Matter* 33, 265402 (2021).
- [20] S. K. Adhikari, *J. Phys.: Condens. Matter* 33, 425402 (2021).
- [21] L. Chomaz, S. Baier, D. Petter, M. J. Mark, F. Wächtler, L. Santos, and F. Ferlaino, *Phys. Rev. X* 6, 041039 (2016).
- [22] F. Wächtler and L. Santos, *Phys. Rev. A* 94, 043618 (2016).
- [23] R. N. Bisset, R. M. Wilson, D. Baillie, and P. B. Blakie, *Phys. Rev. A* 94, 033619 (2016).
- [24] T. D. Lee, K. Huang, and C. N. Yang, *Phys. Rev.* 106, 1135 (1957).
- [25] A. R. P. Lima and A. Pelster, *Phys. Rev. A* 84, 041604(R) (2011).
- [26] A. R. P. Lima and A. Pelster, *Phys. Rev. A* 86, 063609 (2012).
- [27] G. Semeghini, G. Ferioli, L. Masi, C. Mazzinghi, L. Wolswijk, F. Minardi, M. Modugno, G. Modugno, M. Inguscio, and M. Fattori, *Phys. Rev. Lett.* 120, 235301 (2018).
- [28] C. R. Cabrera, L. Tanzi, J. Sanz, B. Naylor, P. Thomas, P. Cheiney, and L. Tarruell, *Science* 359, 301 (2018).
- [29] I. Ferrier-Barbut, H. Kadau, M. Schmitt, M. Wenzel, and T. Pfau, *Phys. Rev. Lett.* 116, 215301 (2016).
- [30] L. Chomaz, D. Petter, P. Ilzhöfer, G. Natale, A. Trautmann, C. Politi, G. Durastante, R. M. W. van Bijnen, A. Patscheider, M. Sohmen, M. J. Mark, and F. Ferlaino, *Phys. Rev. X* 9, 021012 (2019).
- [31] G. Natale, R. M. W. van Bijnen, A. Patscheider, D. Petter, M. J. Mark, L. Chomaz, and F. Ferlaino, *Phys. Rev. Lett.* 123, 050402 (2019).
- [32] L. Tanzi, E. Lucioni, F. Famà, J. Catani, A. Fioretti, C. Gabbanini, R. N. Bisset, L. Santos, and G. Modugno, *Phys. Rev. Lett.* 122, 130405 (2019).
- [33] F. Böttcher, J.-N. Schmidt, M. Wenzel, J. Hertkorn, M. Guo, T. Langen, and T. Pfau, *Phys. Rev. X* 9, 011051 (2019).
- [34] M. Guo, F. Böttcher, J. Hertkorn, J.-N. Schmidt, M. Wenzel, H. P. Büchler, T. Langen, and T. Pfau, *Nature (London)* 574, 386 (2019).
- [35] L. Tanzi, S. Rocuzzo, E. Lucioni, F. Famà, A. Fioretti, C. Gabbanini, G. Modugno, A. Recati, and S. Stringari, *Nature (London)* 574, 382 (2019).
- [36] R. Bombin, J. Boronat, and F. Mazzanti, *Phys. Rev. Lett.* 119, 250402 (2017).
- [37] M. A. Norcia, C. Politi, L. Klaus, E. Poli, M. Sohmen, M. J. Mark, R. Bisset, L. Santos, and F. Ferlaino, *Nature (London)* 596, 357 (2021).
- [38] E. Poli, T. Bland, C. Politi, L. Klaus, M. A. Norcia, F. Ferlaino, R. N. Bisset, and L. Santos, *Phys. Rev. A* 104, 063307 (2021).
- [39] D. Baillie and P. B. Blakie, *Phys. Rev. Lett.* 121, 195301 (2018).
- [40] Y.-C. Zhang, T. Pohl, F. Maucher, *Phys. Rev. A* 104, 013310 (2021).
- [41] J. Hertkorn, J.-N. Schmidt, M. Guo, F. Böttcher, K. S. H. Ng, S.D. Graham, P. Uerlings, T. Langen, M. Zwierlein, and T. Pfau, *Phys. Rev. Research* 3, 033125 (2021).
- [42] Y.-C. Zhang, F. Maucher, and T. Pohl, *Phys. Rev. Lett.* 123, 015301 (2019).
- [43] J. Hertkorn, J.-N. Schmidt, M. Guo, F. Böttcher, K. S. H. Ng, S. D. Graham, P. Uerlings, H. P. Büchler, T. Langen, M. Zwierlein, and T. Pfau, *Phys. Rev. Lett.* 127, 155301 (2021).
- [44] J. Léonard, A. Morales, P. Zupancic, T. Esslinger, and T. Donner, *Nature (London)* 543, 87 (2017).
- [45] T. Lahaye, C. Menotti, L. Santos, M. Lewenstein, and T. Pfau, *Rep. Prog. Phys.* 72, 126401 (2009).
- [46] R. Kishor Kumar, L. E. Young-S., D. Vudragović, A. Balaž, P. Muruganandam, and S. K. Adhikari, *Comput. Phys. Commun.* 195, 117 (2015).
- [47] V. I. Yukalov, *Laser Phys.* 28, 053001 (2018).
- [48] V. Lončar, L. E. Young-S., S. Škrbić, P. Muruganandam, S. K. Adhikari, and A. Balaž, *Comput. Phys. Commun.* 209, 190 (2016).
- [49] P. Muruganandam and S. K. Adhikari, *Comput. Phys. Commun.* 180, 1888 (2009).
- [50] Y. Tang, A. Sykes, N. Q. Burdick, J. L. Bohn, and B. L. Lev, *Phys. Rev. A* 92, 022703 (2015).
- [51] M. D’Onofrio, P. Marziani, and C. Chiosi, *Front. Astron. Space Sci.* 8, 694554 (2021).